

Evaluation Metrics and Methods for Generative Models in the Wireless PHY Layer

Michael Baur¹, Graduate Student Member, IEEE, Nurettin Turan¹, Graduate Student Member, IEEE, Simon Wallner¹, and Wolfgang Utschick¹, Fellow, IEEE

¹TUM School of Computation, Information and Technology, Technical University of Munich, Germany

Corresponding author: Michael Baur (email: mi.baur@tum.de).

M. Baur and N. Turan contributed equally to this work. This work is funded by the Bavarian Ministry of Economic Affairs, Regional Development, and Energy as part of the project 6G Future Lab Bavaria. The authors acknowledge the financial support from the Federal Ministry of Education and Research of Germany, project ID: 16KISK002.

ABSTRACT Generative models are typically evaluated by direct inspection of their generated samples, e.g., by visual inspection in the case of images. Further evaluation metrics like the Fréchet inception distance or maximum mean discrepancy are intricate to interpret and lack physical motivation. These observations make evaluating generative models in the wireless PHY layer non-trivial. This work establishes a framework consisting of evaluation metrics and methods for generative models applied to the wireless PHY layer. The proposed metrics and methods are motivated by wireless applications, facilitating interpretation and understandability for the wireless community. In particular, we propose a spectral efficiency analysis for validating the generated channel norms and a codebook fingerprinting method to validate the generated channel directions. Moreover, we propose an application cross-check to evaluate the generative model's samples for training machine learning-based models in relevant downstream tasks. Our analysis is based on real-world measurement data and includes the Gaussian mixture model, variational autoencoder, diffusion model, and generative adversarial network as generative models. Our results under a fair comparison in terms of model architecture indicate that solely relying on metrics like the maximum mean discrepancy produces insufficient evaluation outcomes. In contrast, the proposed metrics and methods exhibit consistent and explainable behavior.

INDEX TERMS PHY layer, generative model, wireless applications, evaluation metrics.

I. Introduction

LEARNING environment-specific features by training neural networks (NNs) on data from a particular radio propagation environment (RPE) recently emerged as a disruptive paradigm for the development of future wireless systems [1]. The development of novel wireless algorithms based on machine learning (ML) has reached a mature stage and has also found its way into standardization [2]. Methods such as CsiNet exemplarily stand for the success of ML-based wireless systems, enabling an efficient feedback design for frequency division duplex (FDD) systems [3]. Other application examples from the wireless PHY layer include channel estimation [4]–[6] or precoding [7].

Generative models are among the most popular ML-based techniques as they enable learning data distributions based on samples [8]. After successful training, the generative model

allows for data likelihood evaluation and the creation of entirely new samples that follow the captured distribution. Well-known generative models are: the Gaussian mixture model (GMM) [9], variational autoencoder (VAE) [10], [11], generative adversarial network (GAN) [12], and the diffusion model (DM) [13], the latter currently marking the state-of-the-art generation concept in image and speech processing. Most of these models are originally proposed to generate natural signals such as images or speech. Still, they generally work well for arbitrary data and can also be utilized for inference tasks. Thus, generative models also find their way into the wireless literature due to their ability to model complex data relationships. For example, a generative model can build the foundation of an improved network management framework [14]. A generative model can also be used to design a semantics-aware vehicular

network [15]. For the wireless PHY layer, generative models demonstrate great potential in typical applications as well. Channel estimation, categorized as an inverse problem, is a domain where generative models are heavily applied to achieve remarkable estimation quality [16]–[24]. Moreover, generative models are also promising tools for model order selection [25], feedback and precoder design [26], channel prediction [27], or channel modeling [28]–[30].

Almost all of the generative model-based wireless methods above are utilized for inference tasks after their training and not for generating samples. Most methods’ performance is determined by assessing how well the generative model-based approach performs in a follow-up task, e.g., channel estimation. Indeed, in the wireless literature, there is a shortcoming concerning the direct evaluation of a generative model based on its generated samples. This observation contrasts other research disciplines, like image processing, where a fundamental aspect of a generative model’s performance evaluation involves the quality of a generated sample, e.g., by visually inspecting a generated image. Therein, metrics like the Fréchet inception distance (FID) [31] or maximum mean discrepancy (MMD) [32] are two well-known metrics to evaluate a generative model directly on its generated samples. Obviously, there is no such thing as visual quality for wireless data, necessitating alternative means of evaluation. A step in this direction is done by the channel modeling methods in [28]–[30] as they evaluate specific channel parameters like power or delay spread based on the generated channels and compare them with the original data. In [29], the authors go further and train an autoencoder (AE)-based method for channel compression on generated samples. They compare the AE’s performance with an equivalent architecture AE that was trained on the (synthetic) RPE data to quantify the distributional shift between the RPE and generative model channel distributions.

However, the task-specific evaluation for generative models in channel modeling only takes into account the methods proposed in the respective works and does not consider a broad evaluation of other generative models since this is not within the scope of their work. Moreover, the task-specific measures rely on knowing existing channel model parameters, which need to be estimated for measured data from a particular RPE, limiting the validity of a channel parameter comparison. As a result, there is no clear guideline for assessing the quality of a generated channel with an established metric. Therefore, we propose a framework consisting of several evaluation metrics and methods for generative models in this work that are specifically suited for wireless channel data. We perform an extensive usage of the proposed metrics by applying them to the most popular generative models for PHY layer algorithms, i.e., the GMM, VAE, GAN, and DM. Moreover, the evaluation is done for real-world measurement data. The proposed evaluation metrics are motivated by PHY layer applications and have an interpretable character. In particular, the first evaluation metric we

propose compares the achieved spectral efficiency (SE) from the RPE and generated samples marking the information-theoretic transmission bound. Second, we introduce a so-called *codebook fingerprint*, where each dataset has a distinct fingerprint in terms of a codebook typically used in limited feedback schemes [33]. The codebook fingerprint allows for an immediate distinction between channel datasets by visualizing them as discrete probability distributions as a consequence of normalizing empirically obtained histograms and utilizing the total variation distance (TVD) as a distance measure. Third, we propose an application cross-check where a model is trained on RPE data, and another model is trained on generated data from a generative model that was trained on RPE data. Afterward, both models are evaluated for the same task to determine how well the generative model can convey its channel distribution knowledge. Accordingly, the application cross-check provides a general framework where the specific task of interest can be customized. We summarize the primary *contributions* as follows:

- We give an overview of the state-of-the-art generative models for wireless applications and evaluate all of them on the proposed evaluation metrics in a fair comparison in terms of the models’ architectures based on real-world measurements.
- We propose an SE analysis and codebook fingerprinting as evaluation routines, allowing us to assess whether the generative model can capture two important channel properties for PHY layer algorithms: the overall channel power and directional information.
- We introduce a general framework for an application cross-check. The cross-check enables us to determine if a generative model can be utilized in place of the true RPE data for training ML-based PHY layer methods and generate authentic channels.

To the best of our knowledge, our work is the first to establish general evaluation routines for generative models tailored specifically toward wireless PHY layer applications. The routines are easy to implement and interpret yet expressive enough to yield a reliable performance measure. Moreover, our extensive simulations show that, overall, the GMM achieves the best generative quality followed by the VAE. A possible explanation for this behavior is that a GMM or VAE can explicitly incorporate structural knowledge, such as a Toeplitz covariance matrix for uniformly structured arrays [34]. The GAN or DM need to learn this from scratch, an obvious disadvantage. However, we note that this outcome depends on the considered system configuration and that other system layouts may result in different rankings, requiring a system-specific evaluation.

This paper is organized as follows. In Section II, we give an overview of the state-of-the-art generative models for wireless applications, i.e., the GMM, VAE, DM, and GAN. In Section III, we introduce the proposed evaluation metrics and methods for generative models in the wireless

Algorithm 1 Sampling from a GMM.

Require: GMM with parameters $\theta = \{\pi_k, \mu_k, C_k\}_{k=1}^K$, number of samples to generate M .

- 1: **for** $m = 1, \dots, M$ **do**
- 2: $k \sim \text{Cat}([\pi_1, \dots, \pi_K])$
- 3: $\varepsilon \sim \mathcal{N}_{\mathbb{C}}(\mathbf{0}, \mathbf{I})$
- 4: $\tilde{\mathbf{h}}_m \leftarrow \mu_k + C_k^{1/2} \varepsilon$
- 5: **end for**
- 6: **return** GMM generated dataset $\{\tilde{\mathbf{h}}_m\}_{m=1}^M$.

PHY layer. In Section IV, we describe the conducted measurement campaign, followed by the simulation results. We conclude this work in Section V. In Appendix A, we list implementation details.

II. Generative Model Preliminaries

The problem in contemporary generative modeling is to learn a data distribution based on samples to create novel samples that follow the same distribution. More precisely, a generative model utilizes a set of training data samples $\{\mathbf{h}_i\}_{i=1}^{T_r} \subset \mathbb{C}^N$ with $\mathbf{h} \sim p(\mathbf{h})$ to learn $p(\mathbf{h})$ with a parametric approximation $p_{\theta}(\mathbf{h})$. The vector θ contains all the model parameters to specify the learned distribution, e.g., the NN weights. One of the simplest methods to obtain θ is to assume a Gaussian distribution for \mathbf{h}_s , i.e., $\mathbf{h} \sim \mathcal{N}_{\mathbb{C}}(\mu_s, C_s)$ with the sample mean $\mu_s = \frac{1}{T_r} \sum_{i=1}^{T_r} \mathbf{h}_i$ and sample covariance $C_s = \frac{1}{T_r} \sum_{i=1}^{T_r} (\mathbf{h}_i - \mu_s)(\mathbf{h}_i - \mu_s)^H$ such that $\theta = \{\mu_s, C_s\}$. We will refer to it as *scov* in this work. An apparent disadvantage of the scov model is its limited expressiveness due to the single mean and covariance. An elegant way to obtain a more expressive generative model is to let the Gaussian distribution only hold conditionally, enforcing a conditionally Gaussian (CG) model. In particular, the CG likelihood model becomes

$$\mathbf{h} | z \sim p_{\theta}(\mathbf{h} | z) = \mathcal{N}_{\mathbb{C}}(\mathbf{h}; \mu_{\theta}(z), C_{\theta}(z)) \quad (1)$$

with the latent vector $z \in \mathbb{R}^{N_L}$ following a prior $p(z)$. To acquire θ , a likelihood optimization-based approach is typically adopted to maximize $p_{\theta}(\mathbf{h})$.

A. Gaussian Mixture Model

When the condition is a discrete random variable (RV), the number of Gaussian distributions in (1) becomes finite. Therefore, the corresponding likelihood function reads as

$$p_{\theta}(\mathbf{h}) = \sum_{k=1}^K \pi_k \mathcal{N}_{\mathbb{C}}(\mathbf{h}; \mu_k, C_k) \quad (2)$$

with the *mixing coefficients* π_k such that $\sum_{k=1}^K \pi_k = 1$ and $\theta = \{\pi_k, \mu_k, C_k\}_{k=1}^K$ describing a GMM [9]. The mean μ_k and covariance C_k belong to the k -th of in total K Gaussian components. The π_k address the components' weighting. Due to the discrete-valued latent space, the posterior or

responsibility can be calculated in closed-form as

$$p_{\theta}(k | \mathbf{h}) = \frac{\pi_k \mathcal{N}_{\mathbb{C}}(\mathbf{h}; \mu_k, C_k)}{\sum_{\ell=1}^K \pi_{\ell} \mathcal{N}_{\mathbb{C}}(\mathbf{h}; \mu_{\ell}, C_{\ell})}. \quad (3)$$

With the training data samples, a GMM can be fitted with the expectation-maximization (EM) algorithm to maximize $p_{\theta}(\mathbf{h})$; cf. [9] for details. The sampling process from a fitted GMM works as follows. First, a discrete realization from a categorical distribution with probabilities according to the mixing coefficients $\{\pi_i\}_{i=1}^K$ is drawn, determining the GMM component. Second, the selected component is sampled as it is typically done for a Gaussian distribution. Algorithm 1 summarizes the procedure for in total M samples.

B. Variational Autoencoder

Although the GMM is a universal approximator when the number of components grows to infinity [35], the GMM fitting process with the EM algorithm and the responsibility evaluation become problematic with both K and N becoming large. The VAE circumvents this problem by adopting (1) with a continuous condition and parameterizing the mapping from z to $\{\mu_{\theta}(z), C_{\theta}(z)\}$ as a NN, making the VAE more suitable for high-dimensional data. However, the VAE-parameterized posterior

$$p_{\theta}(z | \mathbf{h}) = \frac{p_{\theta}(\mathbf{h} | z)p(z)}{\int p_{\theta}(\mathbf{h} | z)p(z)dz} \quad (4)$$

turns out to be intractable due to the continuous latent space, necessitating an approximate Bayesian technique for the model parameter optimization. To this end, the likelihood is decomposed as [18]

$$\log p_{\theta}(\mathbf{h}) = \mathcal{L}_{\theta, \phi}(\mathbf{h}) + \text{D}_{\text{KL}}(q_{\phi}(z | \mathbf{h}) \| p_{\theta}(z | \mathbf{h})) \quad (5)$$

with the evidence lower bound (ELBO)

$$\mathcal{L}_{\theta, \phi}(\mathbf{h}) = \mathbb{E}_{q_{\phi}}[\log p_{\theta}(\mathbf{h} | z)] - \text{D}_{\text{KL}}(q_{\phi}(z | \mathbf{h}) \| p(z)) \quad (6)$$

and the non-negative Kullback-Leibler (KL) divergence

$$\text{D}_{\text{KL}}(q_{\phi}(z | \mathbf{h}) \| p_{\theta}(z | \mathbf{h})) = \mathbb{E}_{q_{\phi}} \left[\log \left(\frac{q_{\phi}(z | \mathbf{h})}{p_{\theta}(z | \mathbf{h})} \right) \right]. \quad (7)$$

We write $\mathbb{E}_{q_{\phi}(z|\mathbf{h})}[\cdot] = \mathbb{E}_{q_{\phi}}[\cdot]$ for notational brevity. In (5), q_{ϕ} is introduced to approximate the posterior (4), becoming apparent by noticing that an ELBO maximization not only maximizes the likelihood but also minimizes (7).

Despite $p_{\theta}(z | \mathbf{h})$ being non-Gaussian according to (4), its approximation is commonly defined as

$$q_{\phi}(z | \mathbf{h}) = \mathcal{N}(z; \mu_{\phi}(\mathbf{h}), \text{diag}(\sigma_{\phi}^2(\mathbf{h}))) \quad (8)$$

and the prior $p(z) = \mathcal{N}(\mathbf{0}, \mathbf{I})$ due to optimization purposes involving their simplicity to be sampled from. Moreover, the VAE also implements $q_{\phi}(z | \mathbf{h})$ via a NN. Fig. 1 illustrates the described VAE's working principle. The encoder receives a channel \mathbf{h} as input and maps it to the first two moments of $q_{\phi}(z | \mathbf{h})$, i.e., $\mu_{\phi}(\mathbf{h})$ and $\sigma_{\phi}(\mathbf{h})$. Afterward, the *reparameterization trick* is applied to obtain $z = \mu_{\phi}(\mathbf{h}) + \sigma_{\phi}(\mathbf{h}) \odot \varepsilon$. The sample z is the decoder input, being mapped to $\mu_{\theta}(z)$ and $C_{\theta}(z)$ representing the first two moments of $p_{\theta}(\mathbf{h} | z)$.

Algorithm 2 Sampling from a VAE.

Require: VAE decoder NN with parameters θ , number of samples to generate M

- 1: **for** $m = 1, \dots, M$ **do**
- 2: $z \sim \mathcal{N}(\mathbf{0}, \mathbf{I})$
- 3: $\varepsilon \sim \mathcal{N}_{\mathbb{C}}(\mathbf{0}, \mathbf{I})$
- 4: $\tilde{\mathbf{h}}_m \leftarrow \mu_{\theta}(z) + \mathbf{C}_{\theta}^{1/2}(z) \varepsilon$
- 5: **end for**
- 6: **return** VAE generated dataset $\{\tilde{\mathbf{h}}_m\}_{m=1}^M$.

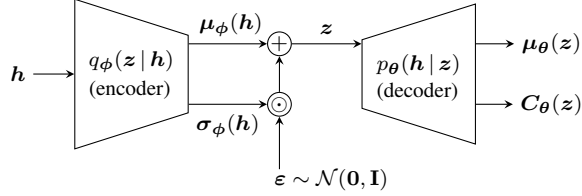


FIGURE 1. Structure of a VAE with CG distributions for $q_{\phi}(z|h)$ and $p_{\theta}(h|z)$. The encoder and decoder each represent a NN.

Furthermore, the CG distributions allow for analytic expressions in the ELBO [18]. Finally, the VAE's sampling process is summarized in Algorithm 2. In step two, the latent vector is drawn from a standard Gaussian distribution. The VAE decoder yields the first two moments of $p_{\theta}(\mathbf{h}|z)$, which are utilized to generate a channel sample in the fourth step.

C. Diffusion Model

The principal concept of the DM is similar to the VAE in the sense they share the ELBO as an optimization objective. Yet, the DM's internal functioning significantly differs from the VAE. The diffusion process involves a repeated addition of noise such that a clean data sample \mathbf{h}_0 becomes pure noise \mathbf{h}_T at the end of the *forward process*, which goes from 0 to T in Fig. 2 and defines a Markov chain [13]. In particular,

$$\mathbf{h}_t = \sqrt{\alpha_t} \mathbf{h}_{t-1} + \sqrt{1 - \alpha_t} \varepsilon, \quad \varepsilon \sim \mathcal{N}(\mathbf{0}, \mathbf{I}) \quad (9)$$

so

$$q(\mathbf{h}_t | \mathbf{h}_{t-1}) = \mathcal{N}(\mathbf{h}_t; \sqrt{\alpha_t} \mathbf{h}_{t-1}, (1 - \alpha_t) \mathbf{I}) \quad (10)$$

with $t = 1, \dots, T$. The time-dependent hyperparameter α_t controls the noise variance in every step and is either learnable or follows a fixed schedule.

To obtain samples with the DM, the *reverse process* represented by $p(\mathbf{h}_{t-1} | \mathbf{h}_t)$ is utilized, which is analytically inaccessible, necessitating an approximation $p_{\theta}(\mathbf{h}_{t-1} | \mathbf{h}_t)$. For determining the structure of $p_{\theta}(\mathbf{h}_{t-1} | \mathbf{h}_t)$, it is beneficial to investigate the DM's ELBO:

$$\begin{aligned} & \mathbb{E}_{q(\mathbf{h}_1 | \mathbf{h}_0)} [\log p_{\theta}(\mathbf{h}_0 | \mathbf{h}_1)] - \text{D}_{\text{KL}}(q(\mathbf{h}_T | \mathbf{h}_0) \| p(\mathbf{h}_T)) \\ & - \sum_{t=2}^T \mathbb{E}_{q(\mathbf{h}_t | \mathbf{h}_0)} [\text{D}_{\text{KL}}(q(\mathbf{h}_{t-1} | \mathbf{h}_t, \mathbf{h}_0) \| p_{\theta}(\mathbf{h}_{t-1} | \mathbf{h}_t))]. \end{aligned} \quad (11)$$

The third term is most relevant for the DM's training as it involves the complete Markov chain except

Algorithm 3 Sampling from a DM.

Require: DM with parameters θ , number of samples to generate M .

- 1: **for** $m = 1, \dots, M$ **do**
- 2: $\mathbf{h} \sim \mathcal{N}(\mathbf{0}, \mathbf{I})$
- 3: **for** $t = T, \dots, 1$ **do**
- 4: $\varepsilon \sim \mathcal{N}(\mathbf{0}, \mathbf{I})$
- 5: $\mathbf{h} \leftarrow \mu_{\theta}(\mathbf{h}, t) + \sigma_t \varepsilon$
- 6: **end for**
- 7: $\tilde{\mathbf{h}}_m \leftarrow \text{real2complex}(\mathbf{h})$
- 8: **end for**
- 9: **return** DM generated dataset $\{\tilde{\mathbf{h}}_m\}_{m=1}^M$.

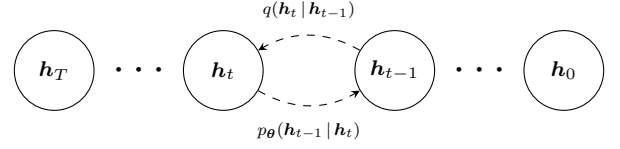


FIGURE 2. Markov chain of the DM involving the forward process with $q(\mathbf{h}_t | \mathbf{h}_{t-1})$ and the approximated reverse process with $p_{\theta}(\mathbf{h}_{t-1} | \mathbf{h}_t)$.

for one step, while the first term is usually neglected, and the second term is assumed to be zero. Consequently, $p_{\theta}(\mathbf{h}_{t-1} | \mathbf{h}_t)$ should be structurally equal to $q(\mathbf{h}_{t-1} | \mathbf{h}_t, \mathbf{h}_0) = \mathcal{N}(\mathbf{h}_{t-1}; \mu_q(\mathbf{h}_t, \mathbf{h}_0), \sigma_t^2 \mathbf{I})$ for an ELBO maximization, resulting in

$$p_{\theta}(\mathbf{h}_{t-1} | \mathbf{h}_t) = \mathcal{N}(\mathbf{h}_{t-1}; \mu_{\theta}(\mathbf{h}_t, t), \sigma_t^2 \mathbf{I}). \quad (12)$$

The mean $\mu_{\theta}(\mathbf{h}_t, t)$ is learned by a NN and

$$\sigma_t^2 = \frac{(1 - \alpha_t)(1 - \bar{\alpha}_{t-1})}{1 - \bar{\alpha}_t}. \quad (13)$$

represents the time-dependent variance with $\bar{\alpha}_t = \prod_{i=1}^t \alpha_i$.

For a more detailed DM introduction, we refer the reader to [36]. Without loss of generality, we have adopted real-valued distributions in this section. In this case, a channel's real and imaginary parts would be stacked to yield a real-valued \mathbf{h}_0 . We describe the DM's sampling procedure in Algorithm 3. The concept is to sample from a standard Gaussian distribution and then repeatedly sample from the reverse process with $p_{\theta}(\mathbf{h}_{t-1} | \mathbf{h}_t)$ until a noise-free sample is reached. In step seven, we indicate that the real-valued sample must be converted to the complex domain at the end.

D. Generative Adversarial Network

The last generative model we discuss in this section is the GAN [12]. A GAN consists of a generator $G_{\theta}(z)$ and a discriminator $D_{\zeta}(\mathbf{h})$, illustrated in Fig. 3, where z is sampled from $\mathcal{N}(\mathbf{0}, \mathbf{I})$. The discriminator's task is to tell whether a sample stems from the true data distribution or the generator, while the generator mimics original data samples as well as possible. This competing behavior is reflected in the GAN's minimax training objective. It is well-known that a GAN

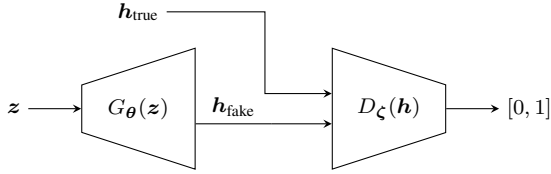


FIGURE 3. Illustration of a GAN with generator $G_{\theta}(z)$ and discriminator $D_{\zeta}(h)$ each representing a NN.

is intricate to train, often suffering from unstable training, mode collapse, or vanishing gradient. Many adaptations have been proposed in the literature to cope with these limitations, of which the Wasserstein GAN (WGAN) is a prominent case [37]. The WGAN’s training strategy reads as

$$\min_{G_{\theta}} \max_{D_{\zeta}} E_{p(h)}[D_{\zeta}(h)] - E_{p(z)}[D_{\zeta}(G_{\theta}(z))] \quad (14)$$

minimizing the Wasserstein-1 distance (W1D). Additionally, a gradient penalty (GP) can be incorporated into the WGAN to improve the generative performance [38]. Since sampling from the WGAN only involves passing z through the generator, we omit a separate sampling algorithm here.

III. Evaluation Metrics and Methods

Evaluation routines for generative models are mainly driven by applications from image or natural language processing. For example, a generative model for image generation is usually evaluated with the generated images’ perceptual quality in combination with metrics like the MMD or FID. Related metrics exist for generated texts, e.g., bilingual evaluation understudy (BLEU) [39]. While visual or auditory inspections are established evaluation routines for corresponding data, such things are problematic regarding wireless channels. Furthermore, metrics like the MMD that can straightforwardly be calculated for channels are themselves a RV without an intuitive meaning, being only suitable in direct comparison to other generated data. Moreover, it is unclear in which way an MMD value can be transferred to the performance in a relevant application. The limited applicability of existing evaluation methods for generative models motivates the proposal of novel techniques specifically tailored toward wireless channels that provide a physical or application-dependent interpretation.

A. Spectral Efficiency Analysis

The quality of a channel realization significantly influences the achievable SE of a communications system, mainly driven by the channel norm. A generative model trained on channel data from a particular RPE should be able to generate channels that produce similarly distributed SEs as the original data. To this end, we evaluate the SE expression

$$r(\mathbf{h}) = \log_2 \left(1 + \frac{\|\mathbf{h}\|_2^2}{\sigma^2} \right) \quad (15)$$

for the system model

$$\mathbf{y} = \mathbf{h} + \mathbf{n}, \quad \mathbf{n} \sim \mathcal{N}_{\mathbb{C}}(\mathbf{0}, \sigma^2 \mathbf{I}). \quad (16)$$

In (15), the channel is either sampled from the original RPE or a generative model to reveal possible differences. For a means of comparing different SE distributions, the empirical cumulative distribution function (CDF) is an appropriate tool for visualization since the SE is one-dimensional. The WID between the RPE and a generated SE distribution, which is the absolute area between the respective CDFs, provides a quantitative measure to support the visual perception.

B. Codebook Fingerprinting

The SE analysis from the previous section primarily contrasts the RPE and generated channels’ norms. For a complete wireless channel comparison, not only the norm but also the channel direction should be taken into account. Channel directions are relevant for many applications, especially precoder design [33]. In FDD systems, the base station (BS) and mobile terminal (MT) typically share a codebook, and the MT only sends the most aligned codebook entry back to the BS for precoding instead of the complete estimated channel to save feedback overhead. More precisely, the codebook $\mathcal{C} = \{c_1, \dots, c_C\}$ representing $B = \log_2 C$ feedback bits is used to determine the feedback index

$$j = \arg \max_n |c_n^H \tilde{\mathbf{h}}|, \quad n = 1, \dots, C \quad (17)$$

for a representative channel sample $\tilde{\mathbf{h}}$.

In a real-world system, $\tilde{\mathbf{h}}$ would be a channel estimate. However, we can also determine the RPE channels’ feedback indices and characterize the directions in the RPE with the codebook. After proper normalization, the result is a discrete probability measure or histogram. Similarly, we can create a histogram for channels sampled from a generative model. Each histogram is representative of the respective channel distribution and yields a *codebook fingerprint*. By comparing different codebook fingerprints with each other, we propose another means of evaluating a generative model for wireless data. Since comparing histograms by inspection is tedious, especially for large codebooks, we additionally compute the TVD between the probability measures. In particular, for the two probability measures P and Q representing the codebook fingerprints, the TVD is given by

$$\delta(P, Q) = \frac{1}{2} \sum_{n=1}^C |P(n) - Q(n)|. \quad (18)$$

The TVD has the beneficial property that it lies between zero and one, where zero attests to a perfect match.

C. Application Cross-Check

As a third way of evaluating a generative model’s quality, we want to investigate how well it can transfer its knowledge to other data-driven methods, e.g., for channel estimation or compression. Concerning knowledge transfer, we mean, what performance gap do we obtain when training a data-driven method on RPE samples compared to training with generative model samples?

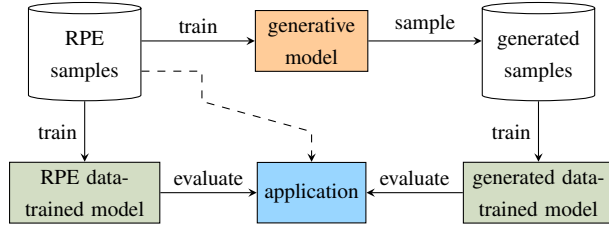


FIGURE 4. Illustration of the application cross-check.

Fig. 4 shows an illustration of the adopted methodology. In the top row, a generative model utilizes RPE samples for its training. Afterward, it generates new generative model samples that should follow the same distribution as the RPE samples. In the bottom row on the left, a data-based model is trained on the RPE samples for a specific application, while on the right, a model is trained on the generative model samples for the same application. The models in the bottom row do not necessarily need to be generative models. They can be any data-based model suitable for the selected application. Nevertheless, the models should be powerful enough to capture their training data distribution. The blue box in the middle symbolizes that the models are evaluated based on the same application with RPE test samples. If the generative model properly learns the RPE distribution, the RPE data-trained model and generated data-trained model in the bottom row should perform similarly on the considered application since the distributional shift between the RPE and generated samples becomes negligible.

As application blocks for Fig. 4, we choose channel estimation and compression for the system model in (16); two PHY layer applications where deep learning (DL) methods are heavily used to improve the performance of a wireless communications system. Accurate channel estimates are vital to attaining the full potential of massive multiple-input multiple-output (MIMO) systems, so channel estimators that are powerful while exhibiting a low computational complexity are essential. What is more, channel compression is relevant for FDD systems to reduce the feedback overhead after the channel has been estimated. To this end, we briefly describe the adopted channel estimators and the channel compression framework for the application cross-check in the following two subsections.

1) Channel Estimators

One of the simplest channel estimators adopts a Gaussian prior and utilizes the sample mean $\boldsymbol{\mu}_s$ and sample covariance matrix \mathbf{C}_s to parameterize a linear minimum mean squared error (LMMSE) estimator. In particular, the estimator reads as

$$\hat{\mathbf{h}}_{\text{scov}}(\mathbf{y}) = \boldsymbol{\mu}_s + \mathbf{C}_s(\mathbf{C}_s + \sigma^2\mathbf{I})^{-1}(\mathbf{y} - \boldsymbol{\mu}_s) \quad (19)$$

for the system model in (16).

A more powerful estimator can be obtained by fitting a GMM prior to the channel distribution and deriving an

estimator aiming at minimizing the mean squared error (MSE) [16]. To compute the final estimate, this GMM-based channel estimator requires a GMM for \mathbf{y} . For this purpose, a GMM is initially fitted for \mathbf{h} according to (2). Then, the GMM is updated with the help of (16) to yield

$$p_{\boldsymbol{\theta}}(\mathbf{y}) = \sum_{k=1}^K \pi_k \mathcal{N}_{\mathbf{C}}(\mathbf{y}; \boldsymbol{\mu}_k, \mathbf{C}_k + \sigma^2\mathbf{I}). \quad (20)$$

with the same $\boldsymbol{\mu}_k$ and \mathbf{C}_k as in (2) and σ^2 as additional parameter. The resulting channel estimate adopting the GMM prior is calculated as

$$\hat{\mathbf{h}}_{\text{GMM}}(\mathbf{y}) = \sum_{k=1}^K p_{\boldsymbol{\theta}}(k | \mathbf{y}) [\boldsymbol{\mu}_k + \mathbf{C}_k(\mathbf{C}_k + \sigma^2\mathbf{I})^{-1}(\mathbf{y} - \boldsymbol{\mu}_k)] \quad (21)$$

with

$$p_{\boldsymbol{\theta}}(k | \mathbf{y}) = \frac{\pi_k \mathcal{N}_{\mathbf{C}}(\mathbf{y}; \boldsymbol{\mu}_k, \mathbf{C}_k + \sigma^2\mathbf{I})}{\sum_{\ell=1}^K \pi_{\ell} \mathcal{N}_{\mathbf{C}}(\mathbf{y}; \boldsymbol{\mu}_{\ell}, \mathbf{C}_{\ell} + \sigma^2\mathbf{I})}. \quad (22)$$

For details regarding the GMM-based estimator derivation, we refer to [16].

Another channel estimator leveraging a powerful generative prior is the VAE-based channel estimator [18]. This approach trains a VAE as in Fig. 1 with the distinction that the encoder receives \mathbf{y} as input since \mathbf{h} is inaccessible during the estimation phase. After its training, the VAE parameterizes $\mathbf{h} | \mathbf{z}$ as CG, which can be exploited to derive an estimator that minimizes the MSE adopting the VAE prior, cf. [18] for details. The resulting VAE-based channel estimator reads as

$$\hat{\mathbf{h}}_{\text{VAE}}(\mathbf{y}) = \boldsymbol{\mu}_{\boldsymbol{\theta}}(\tilde{\mathbf{z}}) + \mathbf{C}_{\boldsymbol{\theta}}(\tilde{\mathbf{z}})(\mathbf{C}_{\boldsymbol{\theta}}(\tilde{\mathbf{z}}) + \sigma^2\mathbf{I})^{-1}(\mathbf{y} - \boldsymbol{\mu}_{\boldsymbol{\theta}}(\tilde{\mathbf{z}})) \quad (23)$$

with $\tilde{\mathbf{z}} = \boldsymbol{\mu}_{\phi}(\mathbf{y})$ being the encoder mean and $\boldsymbol{\mu}_{\boldsymbol{\theta}}(\tilde{\mathbf{z}})$ and $\mathbf{C}_{\boldsymbol{\theta}}(\tilde{\mathbf{z}})$ the corresponding decoder mean and covariance matrix, respectively, cf. Fig. 1.

2) Channel Compression

AE models such as CsiNet [3] are the dominant way in the literature for the channel compression task and are essential parts of feedback schemes in FDD systems [2]. To reduce feedback overhead, the AE compresses a channel estimate at the MT by a specific factor ρ . This step is accomplished with the encoder of the AE. Instead of feedbacking the complete channel estimate back to BS, only the compressed version is fed back. At the BS side, the channel estimate is reconstructed with the AE decoder based on the compressed version. The AE architecture is typically trained by minimizing the MSE.

D. Further Evaluation Metrics

In general, many evaluation metrics exist in the literature to evaluate the quality of generated samples [40]. Two of the most popular are the FID and MMD. Essentially, the metrics compute a dimensionality reduction that aims to preserve the

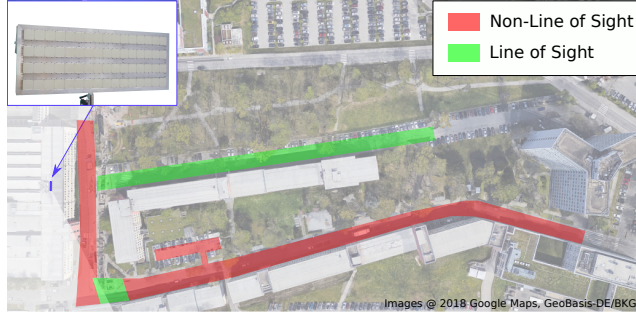


FIGURE 5. Illustration showing the measurement site with the BS at a rooftop and LOS/NLOS conditions for the MT locations [41].

statistical relations between the data. The MMD uses kernels for this task [32], and the FID leverages NNs [31]. We will focus on the MMD in our further elaborations, but similar reasonings hold for the FID.

Closed-form evaluation of the MMD is impractical since only samples are provided for the original data without access to the generating distribution. An unbiased MMD estimate is thus typically computed as

$$\widehat{\text{MMD}}^2(p, q, \phi) = \frac{1}{n(n-1)} \sum_{i \neq j} g_{ij} \quad (24)$$

with $g_{ij} = \phi(\mathbf{p}_i, \mathbf{p}_j) + \phi(\mathbf{q}_i, \mathbf{q}_j) - \phi(\mathbf{p}_i, \mathbf{q}_j) - \phi(\mathbf{q}_i, \mathbf{p}_j)$ based on the samples $\{\mathbf{p}_i\}_{i=1}^L$ and $\{\mathbf{q}_i\}_{i=1}^L$ from the original data distribution p and its approximation q , respectively. The kernel $\phi(\cdot, \cdot)$ is a conventional Gaussian kernel. In our case, p will represent the RPE and q a generative model.

The problem with the MMD is that it is a RV itself with a possible value range between zero and infinity, preventing a direct interpretation. As we will demonstrate in Section IV, the MMD values for different generative models will be comparable. Therefore, calculating the MMD alone to evaluate a generative model would be insufficient, especially for wireless communications-related applications, and should only serve as an auxiliary metric. In contrast, the proposed evaluation metrics and methods from the previous sections are inherently interpretable and allow for an explainable generative model evaluation. In particular, the proposed evaluation metrics also perform a dimensionality reduction similar to the MMD, but towards a well-known quantity like a codebook entry, making it more suitable for wireless communications-related problems.

IV. Evaluation on Real-World Measurement Data

A. Measurement Campaign

As described in [41]–[43], the measurement campaign was conducted at the Nokia campus in Stuttgart, Germany, in 2017. The scenario is displayed in Fig. 5. It can be seen that the measurements were recorded in a street canyon surrounded by buildings producing a mix of line of sight (LOS) and non-line of sight (NLOS) channels. The BS is located on a rooftop approximately 20 m above the ground

with a 10° down-tilt. It is a uniform rectangular array (URA) with $N_v = 4$ vertical and $N_h = 16$ horizontal single polarized patch antennas and was adapted to match the 3rd Generation Partnership Project (3GPP) urban microcell propagation scenario—consequently, $N = 64$. The antenna spacing is λ in the vertical and $\lambda/2$ in the horizontal direction, with λ being the wavelength.

The single monopole receive-antenna representing the MT was placed on a moving vehicle with a maximum speed of 25 km/h. GPS was used to continuously establish synchronization between the BS and MT, yielding a channel realization every 4 mm in space. The data was collected by a TSMW receiver and stored on a Rohde & Schwarz IQR hard disk recorder. The carrier frequency was 2.18 GHz. The BS transmitted 10 MHz orthogonal frequency division multiplexing (OFDM) waveforms with 600 subcarriers in 15 kHz spacing. The pilots were sent continuously with a periodicity of 0.5 ms, arranged in 50 separate subbands of 12 consecutive subcarriers. The channel was assumed to remain constant for one pilot burst. Channel realization vectors with 64 coefficients per subband were extracted in a post-processing step. After the measurement campaign, the normalized mean squared error (NMSE) of the channel estimates was characterized to lie between -20 and -30 dB, reasonably motivating the assumption of possessing perfect channel state information (CSI) for the generative model training.

B. Experiments

This section presents the simulation results based on the real-world measurements from the previous section. We create a dataset of $T_r = 400,000$ channel realizations for the training phases. For evaluation and testing purposes, we consider a $T_v = T_e = 10,000$ channel realizations dataset. The channels are normalized such that $E[\|\mathbf{h}\|^2] = N$. Furthermore, we define the signal-to-noise ratio (SNR) as $\frac{1}{\sigma^2}$ and calculate the NMSE as $\frac{1}{NT_e} \sum_{i=1}^{T_e} \|\mathbf{h}_i - \hat{\mathbf{h}}_i\|^2$ in the experiments, where \mathbf{h}_i and $\hat{\mathbf{h}}_i$ mark the ground-truth channel and its estimate/reconstruction, respectively. We fit a GMM with $K = 64$ components for all experiments as considering more components did not notably improve the performance. For a detailed architecture and training description of the NN-based methods, we refer to Appendix A. Overall, we chose comparable NN architectures regarding layers and model weight numbers to ensure a fair comparison.

1) Spectral Efficiency Analysis

We begin with the SE analysis by comparing the empirical SE CDFs of samples from the RPE and different generative models. To this end, we generate 10,000 channel vector realizations with every generative model as described in Section II and calculate the SE for every realization according to (15). The result at an SNR of 20 dB is displayed in Fig. 6. To increase the validity of this evaluation method, we also

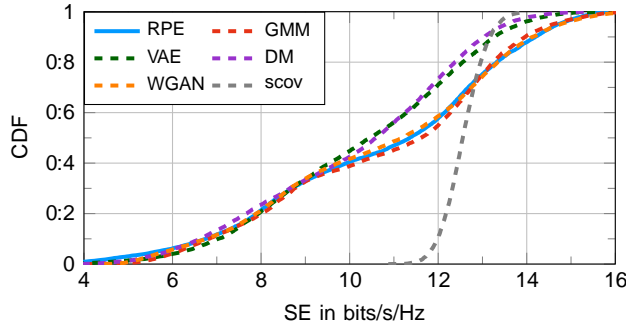


FIGURE 6. Empirical SE CDFs for original samples from the RPE or a generative model. For the corresponding W1D values, see Table 1.

TABLE 1. Evaluation metrics for GM samples compared to RPE samples.

Model	W1D	TVD	MMD
GMM	5:3 10^{-2}	5:6 10^{-2}	7:1 10^{-5}
VAE	1:7 10^{-1}	8:3 10^{-2}	8:7 10^{-3}
DM	1:9 10^{-1}	8:5 10^{-2}	1:2 10^{-2}
WGAN	4:0 10^{-2}	1:0 10^{-1}	4:1 10^{-3}
scov	7:0 10^{-1}	5:2 10^{-1}	3:6 10^{-2}

show the result for the scov model, which is equivalent to a GMM with one component. The figure highlights that the scov model cannot capture the SE characteristics of the RPE. In contrast, the GMM and WGAN SE CDFs are very close to the RPE CDF. The VAE and DM manage to reasonably approximate the RPE CDF for SEs lower than 10 bits/s/Hz and exhibit a moderate deviation for larger SEs.

To quantify the discrepancies between the RPE SE and the respective generative model SEs, we also show the W1D in Table 1 (second column). Every column entry represents the W1D between the RPE SE and respective generative model SE distribution, e.g., the third row between the RPE and VAE. Accordingly, the WGAN produces the best results in terms of the W1D, followed by the GMM. Obviously, the scov has the worst W1D due to the bad SE reproduction. As explained in Appendix A, the WGAN is trained with entry-wise standardization, which is a reason for its good SE reproduction performance.

2) Codebook Fingerprinting

The SE analysis focuses on a generative model's channel norm reproduction capability. To also investigate the reproduction capability of the channel directions, we will make use of the proposed codebook fingerprinting evaluation routine. As for the SE analysis, we create 10,000 channel realizations with every generative model for comparison with the RPE test dataset. We utilize a codebook consisting of the Kronecker product of two discrete fourier transform (DFT) matrices motivated by the URA at the BS [44]. More precisely, we adopt

$$C = \begin{bmatrix} \mathbf{F}_{C_1}^{(N_v)} & \mathbf{F}_{C_2}^{(N_h)} \end{bmatrix}^0 \quad (25)$$

as codebook where $\mathbf{F}_{C_1}^{(N_v)} \in \mathbb{C}^{N_v \times C_1}$ is a DFT matrix with C_1 columns, and $\mathbf{F}_{C_2}^{(N_h)} \in \mathbb{C}^{N_h \times C_2}$ analogously. We further set $C_1 = 4$ and $C_2 = 16$ to yield a $B = 6$ bits codebook with $C = C_1 C_2 = 64$ entries.

We plot the corresponding codebook fingerprints in Fig. 7, where each generative model is displayed in direct comparison to the RPE. In Fig. 7(a), we show the GMM codebook fingerprint. As can be seen from the figure, the RPE channel directions are almost wholly represented by the first codebook half, reflecting the inherent characteristics of the RPE. The GMM is very close to the RPE codebook fingerprint. This impression is confirmed by the lowest TVD in Table 1. Additionally, we present the scov codebook fingerprint in Fig. 7(a). The scov approach fails to replicate the RPE codebook fingerprint and exhibits substantial deviations. Recalling that the TVD lies between zero and one, the scov's TVD value in Table 1 is poor.

Moving on, in the remaining codebook fingerprints in Fig. 7, we only display the results of the first codebook half for a finer visualization. The VAE codebook fingerprint in Fig. 7(b) is again close to the RPE, although there are some larger deviations from the RPE after a detailed investigation. We observe a similar trend for the DM in Fig. 7(c), meaning the DM codebook fingerprint also closely approaches the RPE. The TVDs of the VAE and DM in Table 1 validate their similar performance. At last, we investigate the WGAN's codebook fingerprint in Fig. 7(d). In this illustration, we observe some more significant deviations from the RPE, e.g., at codebook entry 20. The WGAN's TVD value in Table 1 is the worst among the considered generative models. Therefore, the GMM is best in replicating the directional information contained in the RPE, followed by the VAE, DM, and WGAN in that order.

3) Application Cross-Check

The third and last evaluation routine we investigate is the application cross-check from Section III-C. We begin with channel estimation as an application by considering the GMM-based and VAE-based channel estimators as explained in Section III-C. To this end, we first train all the considered generative models on the RPE data as described in Appendix A. After the training, we generate a training, validation, and test dataset of the same size as for the RPE with each generative model. The GMM-based and VAE-based channel estimators are then trained on the generated data in the same manner as on the RPE data, including usage of the same number of mixture components and architecture. The GMM is fitted with 64 components, and the VAE has the same architecture as in [43]. Ultimately, all channel estimators are evaluated on the same RPE test dataset to compare their performance.

The performance comparison in terms of the NMSE is presented in Table 2 for an SNR of 10 dB. The NMSEs in the table are scaled by 10^{-2} . Every row in the table is

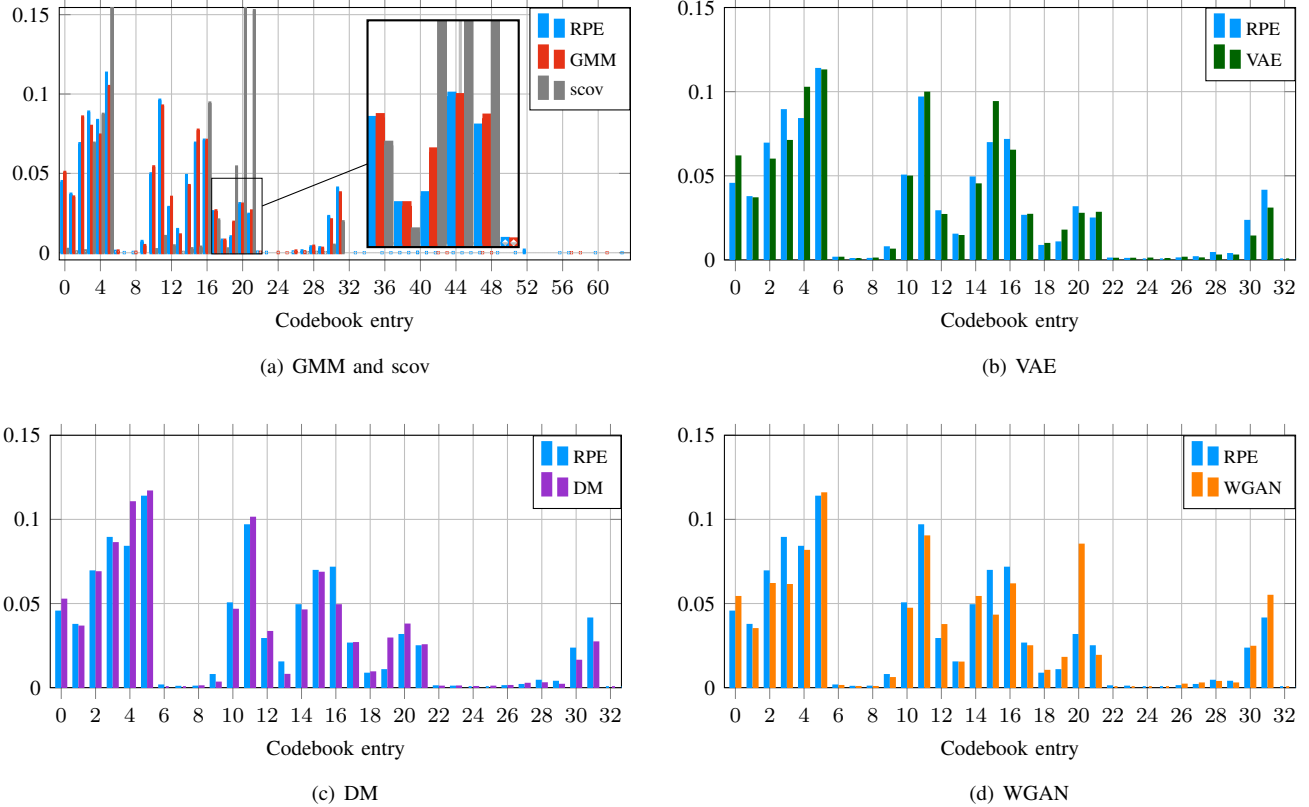


FIGURE 7. Codebook fingerprints for different GM samples compared to RPE samples. Each entry on the x-axis represents a codebook entry, and the corresponding relative frequency is shown on the y-axis. In (a), we show the relative frequencies for the complete codebook. The remaining histograms show only the first half for a more detailed exposition. For the corresponding TVD values, see Table 1.

TABLE 2. NMSEs ($\cdot 10^{-2}$) for different GM-based channel estimators.

		Sample distribution					
Estimator	Method	RPE	GMM	scov	VAE	DM	WGAN
	GMM	2.83	2.90	5.64	3.20	3.40	5.13
	VAE	3.38	3.68	6.11	3.97	4.07	4.85
	LMMSE	5.62	5.62	5.65	5.87	6.01	6.56

assigned to a channel estimator. Every column describes the data origin for the “generated data-trained model” in Fig. 4. For instance, the entry in row “VAE” and column “DM” represents the NMSE of the VAE-based channel estimator that is trained with data from the DM as a generative model. The NMSEs in the column “RPE” belong to the “RPE data-trained model” in Fig. 4, where the channel estimator in the corresponding table row is trained on the RPE data. So, the other column entries should replicate the NMSEs in the “RPE” column for the best result.

Throughout all channel estimation experiments, the GMM reproduces the “RPE” NMSE best. For the “GMM” row, the strong performance can be partly attributed to fitting the GMM-based estimator to GMM-distributed data, which might be seen as an unfair advantage for the GMM as a generative model. Thus, the result in the “VAE” column is

important to highlight that the GMM as a generative model also performs very well when the estimator is not GMM-distributed, confirming the GMM’s great performance also in this case. The second best generator with the GMM and VAE as estimators is the VAE followed by the DM. In the last row of Table 2, we also display the NMSE when using a simple LMMSE estimator with sample mean and covariance matrix as channel estimator, cf. (19). The LMMSE row highlights that the channel estimator should be powerful enough to learn a good estimate of the RPE distribution since, in this row, using the scov method for generation performs very closely to the “RPE” column, limiting the expressiveness of the result. Additionally, we present the performance of the GMM-based channel estimator over the SNR for the considered generative models in Fig. 8. We qualitatively observe the same behavior in this plot as for the “GMM” row in Table 2 since the GMM performs again best, followed by the VAE and DM. It is also visible that the WGAN shows the poorest performance among the generative models.

We continue with the cross-check with channel compression as an application. To this end, we exchange the “application” block in Fig. 4 with channel compression and leave the remainder as in the channel estimation check. We train an AE where both the encoder and decoder are five-

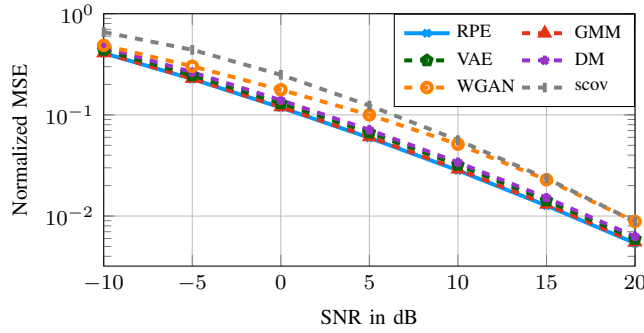


FIGURE 8. Application cross-check with the GMM channel estimator.

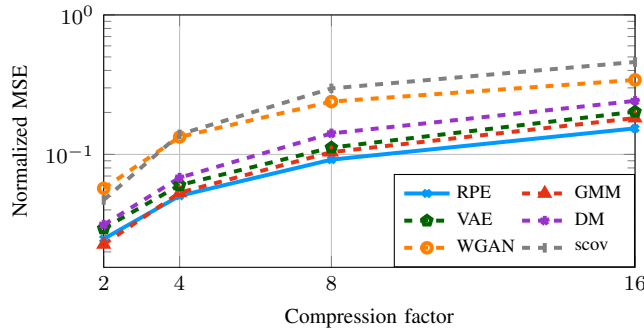


FIGURE 9. Application cross-check with the AE for channel compression.

layer NNs. Every encoder layer consists of a convolutional layer with kernel size 9 and 64 convolutional channels, a batch normalization layer, and a ReLU activation function. The channel is downsampled until a compression factor of ρ is reached while we consider $\rho \in \{2, 4, 8, 16\}$. For the encoder input, the channel is first transformed to the beamspace, and then real and imaginary parts are the two input convolutional channels. The decoder is a symmetrical version of the encoder and upsamples the compressed channel until the original dimensionality is reached. This architecture is equivalent for every considered generative model training data. Fig. 9 presents the simulation results for the channel compression cross-check. Again, the GMM is closest to the RPE performance, followed by the VAE, DM, and WGAN. This result aligns with the results from the previous cross-check regarding channel estimation.

At last, we want to take a look at the rightmost column of Table 1 where the MMDs between RPE samples and the considered generative model samples are listed. It can be seen that the GMM also achieves the best value in this comparison, with the WGAN and VAE being the second and third best, respectively. However, the table also highlights that the MMD is intricate to interpret, and relying on the MMD alone as an evaluation metric is insufficient. This can be deduced by comparing the MMD value for the DM and scov. The values lie closely together, although the DM achieves significantly better generation results as the

scov in all of our proposed evaluation routines. Moreover, the WGAN has the second best MMD value, which might be misleading since the WGAN performed worst in the codebook fingerprinting and application cross-check among the considered generative models. These findings emphasize the importance of application-motivated evaluation routines for wireless data, as existing evaluation methods like the MMD might produce misleading results.

V. Concluding Remarks and Future Work

In this work, we propose evaluation metrics and methods for generative models tailored toward wireless PHY layer data. The considered methods involve an SE comparison, a codebook fingerprinting, and an application cross-check. We consider popular generative models in the wireless literature in our evaluation based on real-world measurements, which include the GMM, VAE, DM, and WGAN. Our results indicate that solely relying on established metrics in the ML literature, e.g., the MMD, is insufficient and that wireless data requires evaluation routines motivated by wireless applications. To the best of our knowledge, our proposed evaluation metrics and methods provide the first framework for establishing evaluation routines for generative models in the wireless PHY layer.

We note that the results in this work depend on the system configuration and the considered RPE represented by the measurement data. Depending on the system constraints as well as the dataset characteristics, the rankings of the generative models in Section IV might change. Indeed, the scope of this work is not to determine the best generative model but to establish general evaluation metrics and methods for generative models in the wireless PHY layer, which exhibit a connection to relevant applications. In future works, we want to extend the evaluation framework with the proposed routines by considering different typical PHY layer applications with various system constraints, such as a limited training dataset size, corrupted training data samples, model memory requirements, and online computational complexity.

Appendix

A. Implementation Details

We implement all the NN architectures with the help of *PyTorch* and also follow the PyTorch nomenclature in describing the layers. That means the first argument in a convolutional layer refers to the input convolutional channels, the second to the output convolutional channels, etc. The same reasoning holds for all other layers.

1) VAE Implementation

The VAE architecture for generation is similar to the architecture in [43]. Thus, we parameterize $C_\theta(z)$ as a block-Toeplitz matrix in alignment with the URA, i.e.,

$$C_\theta(z) = Q^H \text{diag}(c_\theta(z))Q, \quad c_\theta(z) \in \mathbb{R}^{4N}, \quad (26)$$

TABLE 3. Architecture details of the implemented VAE.

#	encoder	decoder
0	Conv1d(2, 16, 1, 1)	Linear(16, 1225)
	-	Reshape(-1, 49, 25)
1	Conv1d(16, 16, 11, 2, 1)	ConvTranspose1d(49, 28, 11, 2, 1)
	BatchNorm1d(16)	BatchNorm1d(49)
	ReLU()	ReLU()
2	Conv1d(16, 28, 11, 2, 1)	ConvTranspose1d(28, 16, 11, 2, 1)
	BatchNorm1d(28)	BatchNorm1d(16)
	ReLU()	ReLU()
3	Conv1d(28, 49, 11, 2, 1)	ConvTranspose1d(16, 3, 11, 2, 1)
	BatchNorm1d(49)	BatchNorm1d(3)
	ReLU()	ReLU()
4	Flatten(1)	Flatten(1)
	Linear(1225, 32)	Linear(747, 384)

where $\mathbf{Q} = \mathbf{F}_{N_v}^{(2N_v)} \otimes \mathbf{F}_{N_h}^{(2N_h)}$ is the Kronecker product of two two-times oversampled DFT-matrices. Table 3 separately displays the encoder and decoder architecture, where the left-most column shows the layer number. The encoder receives \mathbf{h} as input, with the real and imaginary parts forming the two input convolutional channels. We additionally transform the encoder input to the beamspace as this benefitted the training in previous works [18]. The dimensionality of the latent space is set to $N_L = 16$, and we use an exponential function to map to strictly positive values for σ_ϕ and c_θ . For the model weight optimization, we utilize the Adam optimizer with a learning rate of 0.0001. The model weights are optimized until saturation of the ELBO on the validation dataset is reached.

2) DM Implementation

For the DM implementation, we make use of the simulation code from [24] and increase the number of model weights such that a similar number as in the VAE from Table 3 is reached. Table 4 gives an overview of the DM layers, which are split into a net-pre and a net-post. The convolutional layers perform a *same* convolution. As displayed in [24, Fig. 1], the network for the reverse process is split into two parts (net-pre and net-post here). After the net-pre, the positional embedding for t is incorporated into the net-pre output. Then, the composition is processed by the net-post to yield $\mu_\theta(\mathbf{h}_t, t)$, cf. (12). Moreover, the number of diffusion steps is set to $T = 1000$ here. Apart from that, the training procedure of the DM is identical to [24], where the Adam optimizer with an initial learning rate of 0.0005 is used that is step-wise decreased. The DM is trained for up to 500 epochs or until it saturates on the validation dataset.

3) WGAN Implementation

The WGAN implementation follows the simulation code from [22], which includes considering the GP for the

TABLE 4. Architecture details of the implemented DM.

#	net-pre	net-post
0	Conv1d(2, 26, 7)	Conv1d(128, 102, 7)
	ReLU()	ReLU()
1	Conv1d(26, 51, 7)	Conv1d(102, 77, 7)
	ReLU()	ReLU()
2	Conv1d(51, 77, 7)	Conv1d(77, 51, 7)
	ReLU()	ReLU()
3	Conv1d(77, 102, 7)	Conv1d(51, 26, 7)
	ReLU()	ReLU()
4	Conv1d(128, 102, 7)	Conv1d(26, 2, 7)

TABLE 5. Architecture details for the implemented WGAN.

#	generator	discriminator
0	Linear(32, 2048)	Conv1d(2, 16, 3)
	ReLU()	MaxPool1d(3, 2)
	View(-1, 128, 16)	LeakyReLU(0.2)
	Upsample(None, 2.0)	Dropout(0.25)
1	Conv1d(128, 128, 4)	Conv1d(16, 32, 3)
	BatchNorm1d(128)	MaxPool1d(3, 2)
	ReLU()	LeakyReLU(0.2)
	Upsample(None, 2.0)	Dropout(0.25)
2	Conv1d(128, 128, 4)	Conv1d(32, 64, 3)
	BatchNorm1d(128)	MaxPool1d(3, 2)
	ReLU()	LeakyReLU(0.2)
	-	Dropout(0.25)
3	Conv1d(128, 2, 4)	Conv1d(64, 128, 3)
	-	LeakyReLU(0.2)
	-	Dropout(0.25)
4	-	Flatten(1)
	-	Linear(896, 1)

training. We adapt the sizes of the layers to better fit the dimensionality of our channel realizations, which is 64. Table 5 presents the corresponding architecture, where a latent dimension of 32 is adopted, and *same* convolutions are performed. Additionally, the channel vectors are transformed to the beamspace and standardized per entry as described in [22]. The latter is separately done for the real and imaginary parts such that every entry has a mean zero and variance one since this procedure is reported to improve the WGAN performance [45]. We optimize the generator and discriminator weights with the RMSProp optimizer with a learning rate of 0.0001 for up to 500 epoch or until the validation loss saturates.

REFERENCES

- [1] W. Yu, F. Sofrabi, and T. Jiang, "Role of Deep Learning in Wireless Communications," *IEEE BITS Inf. Theory Mag.*, vol. 2, no. 2, pp. 56–72, 2022.
- [2] 3GPP, "Study on Artificial Intelligence (AI)/Machine Learning (ML) for NR air interface (Release 18)," 3rd Generation Partnership Project (3GPP), Tech. Rep. 38.843 V18.0.0, 2023.
- [3] C. K. Wen, W. T. Shih, and S. Jin, "Deep Learning for Massive MIMO CSI Feedback," *IEEE Wirel. Commun. Lett.*, vol. 7, no. 5, pp. 748–751, 2018.

- [4] H. Ye, G. Y. Li, and B. H. Juang, "Power of Deep Learning for Channel Estimation and Signal Detection in OFDM Systems," *IEEE Wirel. Commun. Lett.*, vol. 7, no. 1, pp. 114–117, 2018.
- [5] D. Neumann, T. Wiese, and W. Utschick, "Learning The MMSE Channel Estimator," *IEEE Trans. Signal Process.*, vol. 66, no. 11, pp. 2905–2917, 2018.
- [6] M. Soltani, V. Pourahmadi, A. Mirzaei, and H. Sheikhzadeh, "Deep Learning-Based Channel Estimation," *IEEE Commun. Lett.*, vol. 23, no. 4, pp. 2019–2022, 2019.
- [7] J. Shi, W. Wang, X. Yi, X. Gao, and G. Y. Li, "Deep Learning-Based Robust Precoding for Massive MIMO," *IEEE Trans. Commun.*, vol. 69, pp. 7429–7443, 2021.
- [8] L. Ruthotto and E. Haber, "An introduction to deep generative modeling," *GAMM-Mitteilungen*, vol. 44, no. 2, p. e202100008, 2021.
- [9] C. M. Bishop, *Pattern Recognition and Machine Learning*. Springer, 2006.
- [10] D. J. Rezende, S. Mohamed, and D. Wierstra, "Stochastic Backpropagation and Approximate Inference in Deep Generative Models," in *Proc. 31st Int. Conf. Mach. Learn.*, 2014.
- [11] D. P. Kingma and M. Welling, "Auto-Encoding Variational Bayes," in *Proc. 2nd Int. Conf. Learn. Represent.*, 2014.
- [12] I. Goodfellow, J. Pouget-Abadie, M. Mirza, B. Xu, D. Warde-Farley, S. Ozair, A. Courville, and Y. Bengio, "Generative Adversarial Networks," *Commun. ACM*, vol. 63, no. 11, pp. 139–144, 2020.
- [13] J. Ho, A. Jain, and P. Abbeel, "Denosing Diffusion Probabilistic Models," *Adv. Neural Inf. Process. Syst.*, vol. 33, 2020.
- [14] Y. Liu, H. Du, D. Niyato, J. Kang, Z. Xiong, D. I. Kim, and A. Jamalipour, "Deep Generative Model and Its Applications in Efficient Wireless Network Management: A Tutorial and Case Study," *IEEE Wirel. Commun.*, pp. 1–9, 2024.
- [15] R. Zhang, K. Xiong, H. Du, D. Niyato, J. Kang, X. Shen, and H. Vincent Poor, "Generative AI-enabled Vehicular Networks: Fundamentals, Framework, and Case Study," *IEEE Netw.*, 2024.
- [16] M. Koller, B. Fesl, N. Turan, and W. Utschick, "An Asymptotically MSE-Optimal Estimator Based on Gaussian Mixture Models," *IEEE Trans. Signal Process.*, vol. 70, pp. 4109–4123, 2022.
- [17] M. Baur, N. Turan, B. Fesl, and W. Utschick, "Channel Estimation in Underdetermined Systems Utilizing Variational Autoencoders," in *2024 IEEE Int. Conf. Acoust. Speech Signal Process.*, 2024, pp. 9031–9035.
- [18] M. Baur, B. Fesl, and W. Utschick, "Leveraging Variational Autoencoders for Parameterized MMSE Estimation," *arXiv preprint arXiv:2307.05352*, 2024.
- [19] B. Fesl, N. Turan, B. Bock, and W. Utschick, "Channel Estimation for Quantized Systems based on Conditionally Gaussian Latent Models," *IEEE Trans. Signal Process.*, vol. 72, pp. 1475–1490, 2024.
- [20] E. Balevi and J. G. Andrews, "Wideband Channel Estimation With a Generative Adversarial Network," *IEEE Trans. Wirel. Commun.*, vol. 20, no. 5, pp. 3049–3060, 2021.
- [21] E. Balevi, A. Doshi, A. Jalal, A. Dimakis, and J. G. Andrews, "High Dimensional Channel Estimation Using Deep Generative Networks," *IEEE J. Sel. Areas Commun.*, vol. 39, no. 1, pp. 18–30, 2021.
- [22] A. S. Doshi, M. Gupta, and J. G. Andrews, "Over-the-Air Design of GAN Training for mmWave MIMO Channel Estimation," *IEEE J. Sel. Areas Inf. Theory*, vol. 3, no. 3, pp. 557–573, 2022.
- [23] M. Arvinte and J. I. Tamir, "MIMO Channel Estimation Using Score-Based Generative Models," *IEEE Trans. Wirel. Commun.*, vol. 22, no. 6, pp. 3698–3713, 2023.
- [24] B. Fesl, M. Baur, F. Strasser, M. Joham, and W. Utschick, "Diffusion-based Generative Prior for Low-Complexity MIMO Channel Estimation," *arXiv preprint arXiv:2403.03545*, 2024.
- [25] M. Baur, F. Weißer, B. Böck, and W. Utschick, "Model Order Selection with Variational Autoencoding," in *2023 IEEE 24th Int. Work. Signal Process. Adv. Wirel. Commun.*. IEEE, 2023, pp. 586–590.
- [26] N. Turan, B. Fesl, M. Koller, M. Joham, and W. Utschick, "A Versatile Low-Complexity Feedback Scheme for FDD Systems via Generative Modeling," *IEEE Trans. Wirel. Commun.*, vol. 23, no. 6, pp. 6251–6265, 2024.
- [27] N. Turan, B. Böck, K. J. Chan, B. Fesl, F. Burmeister, M. Joham, G. Fettweis, and W. Utschick, "Wireless Channel Prediction via Gaussian Mixture Models," in *2024 27th Int. Work. Smart Antennas*. IEEE, 2024, pp. 1–5.
- [28] W. Xia, S. Rangan, M. Mezzavilla, A. Lozano, G. Geraci, V. Semkin, and G. Loianno, "Generative Neural Network Channel Modeling for Millimeter-Wave UAV Communication," *IEEE Trans. Wirel. Commun.*, vol. 21, no. 11, pp. 9417–9431, 2022.
- [29] H. Xiao, W. Tian, W. Liu, and J. Shen, "ChannelGAN: Deep Learning-Based Channel Modeling and Generating," *IEEE Wirel. Commun. Lett.*, vol. 11, no. 3, pp. 650–654, 2022.
- [30] F. Euchner, J. Sanzi, M. Henninger, and S. Ten Brink, "GAN-based Massive MIMO Channel Model Trained on Measured Data," in *2024 27th Int. Work. Smart Antennas*. IEEE, 2024, pp. 109–116.
- [31] M. Heusel, H. Ramsauer, T. Unterthiner, B. Nessler, and S. Hochreiter, "GANs Trained by a Two Time-Scale Update Rule Converge to a Local Nash Equilibrium," *Adv. Neural Inf. Process. Syst.*, vol. 30, 2017.
- [32] A. Gretton, K. M. Borgwardt, M. J. Rasch, B. Schölkopf, and A. Smola, "A Kernel Two-Sample Test," *J. Mach. Learn. Res.*, vol. 13, pp. 723–773, 2012.
- [33] D. Love, R. Heath, V. N. Lau, D. Gesbert, B. Rao, and M. Andrews, "An overview of limited feedback in wireless communication systems," *IEEE J. Sel. Areas Commun.*, vol. 26, no. 8, pp. 1341–1365, 2008.
- [34] B. Fesl, M. Joham, S. Hu, M. Koller, N. Turan, and W. Utschick, "Channel Estimation based on Gaussian Mixture Models with Structured Covariances," in *2022 56th Asilomar Conf. Signals, Syst. Comput.*, 2022, pp. 533–537.
- [35] T. T. Nguyen, H. D. Nguyen, F. Chamroukhi, and G. J. McLachlan, "Approximation by finite mixtures of continuous density functions that vanish at infinity," *Cogent Math. Statist.*, vol. 7, no. 1, p. 1750861, 2020.
- [36] C. Luo, "Understanding Diffusion Models: A Unified Perspective," *arXiv preprint arXiv:2208.11970*, 2022.
- [37] M. Arjovsky, S. Chintala, and L. Bottou, "Wasserstein Generative Adversarial Networks," in *Proc. 34th Int. Conf. Mach. Learn.*, 2017, pp. 214–223.
- [38] I. Gulrajani, F. Ahmed, M. Arjovsky, V. Dumoulin, and A. C. Courville, "Improved Training of Wasserstein GANs," *Adv. Neural Inf. Process. Syst.*, vol. 30, 2017.
- [39] A. Vaswani, N. Shazeer, N. Parmar, J. Uszkoreit, L. Jones, A. N. Gomez, Ł. Kaiser, and I. Polosukhin, "Attention Is All You Need," *Adv. Neural Inf. Process. Syst.*, vol. 30, 2017.
- [40] S. Bischoff, A. Darcher, M. Deistler, R. Gao, F. Gerken, M. Gloeckler, L. Haxel, J. Kapoor, J. K. Lappalainen, J. H. Macke, G. Moss, M. Pals, F. Pei, R. Rapp, A. E. Sağtekin, C. Schröder, A. Schulz, Z. Stefanidi, S. Toyota, L. Ulmer, and J. Vetter, "A Practical Guide to Statistical Distances for Evaluating Generative Models in Science," *arXiv preprint arXiv:2403.12636*, pp. 1–37, 2024.
- [41] C. Hellings, A. Dehmani, S. Wesemann, M. Koller, and W. Utschick, "Evaluation of Neural-Network-Based Channel Estimators Using Measurement Data," in *2019 23rd Int. ITG Work. Smart Antennas*, Vienna, Austria, 2019, pp. 164–168.
- [42] N. Turan, B. Fesl, M. Grundei, M. Koller, and W. Utschick, "Evaluation of a Gaussian Mixture Model-based Channel Estimator using Measurement Data," in *2022 Int. Symp. Wirel. Commun. Syst.*. IEEE, 2022, pp. 1–6.
- [43] M. Baur, B. Böck, N. Turan, and W. Utschick, "Variational Autoencoder for Channel Estimation: Real-World Measurement Insights," in *2024 27th Int. Work. Smart Antennas*. IEEE, 2024, pp. 117–122.
- [44] J. Li, X. Su, J. Zeng, Y. Zhao, S. Yu, L. Xiao, and X. Xu, "Codebook Design for Uniform Rectangular Arrays of Massive Antennas," in *2013 IEEE 77th Veh. Technol. Conf.*. IEEE, jun 2013, pp. 1–5.
- [45] A. Srivastava, C. Russell, L. Valkov, M. U. Gutmann, and C. Sutton, "VEEGAN: Reducing Mode Collapse in GANs using Implicit Variational Learning," *Adv. Neural Inf. Process. Syst.*, vol. 30, 2017.